Theoretical dark matter halo density profile

Eduard Salvador-Solé,[★] Jordi Viñas, Alberto Manrique and Sinue Serra

Institut de Ciències del Cosmos, Universitat de Barcelona (UB–IEEC), Martí i Franquès 1, E-08028 Barcelona, Spain

ABSTRACT

We derive the density profile for collisionless dissipationless dark matter haloes in hierarchical cosmologies making use of the secondary infall (SI) model. The novelties are (i) we deal with triaxial virialized objects, (ii) their seeds in the linear regime are peaks endowed with *unconvolved* spherically averaged density profiles according to the peak formalism, (iii) the initial peculiar velocities are taken into account and (iv) accreting haloes are assumed to develop from the inside out, keeping the instantaneous inner system unaltered. The validity of this latter assumption is accurately checked by comparing analytical predictions on such a growth with the results of numerical simulation. We show that the spherically averaged density profile of virialized objects can be inferred with no need to specify their shape. The *typical* spherically averaged halo density profile is inferred, down to arbitrarily small radii, from the power spectrum of density perturbations. The predicted profile in the Λ cold dark matter cosmology is approximately described by an Einasto profile, meaning that it does not have a cusp but rather a core, where the inner slope slowly converges to zero. Down to one-hundredth the total radius, the profile has the right NFW and Einasto forms, being close to the latter down to a radius of about four orders of magnitude less. The inner consistency of the model implies that the density profiles of haloes harbour no information on their past aggregation history. This would explain why major mergers do not alter the typical density profile of virialized objects formed by SI and do not invalidate the peak formalism based on such a formation.

Key words: methods: analytical – galaxies: haloes – cosmology: theory – dark matter.

1 INTRODUCTION

In the last two decades, observations, and particularly simulations, have provided us with detailed information on the structure and kinematics of bottom-up hierarchically assembled virialized dark matter haloes. However, from the theoretical viewpoint, the situation is far from satisfactory. The way all these properties settle down remains to be elucidated, and their connection with the power spectrum of density perturbations is unknown.

The accurate modelling of virialized self-gravitating collisionless dissipationless systems is an old unresolved issue. Most efforts have focused on determining the equilibrium density profile for objects formed from the monolithic collapse of an isolated spherically symmetric seed with outward-decreasing density profile and pure Hubble velocity field, the so-called secondary infall (SI) model. Following the seminal work by Gunn & Gott (1972), the power-law density profile was derived under the self-similar approximation and/or making use of an adiabatic invariant during virialization, both for pure radial orbits (Gunn 1977; Fillmore & Goldreich 1984;

Bertschinger 1985; Hoffman & Shaham 1985) and non-radial orbits (Ryden & Gunn 1987; White & Zaritsky 1992; Nusser 2001; Le Delliou & Henriksen 2003). The departures from spherical symmetry (by adopting, instead, cylindrical symmetry; Ryden 1993; Moutarde et al. 1995) and self-similarity (Łokas 2000; Łokas & Hoffman 2000) were also investigated.

These theoretical results were tested and complemented by the information drawn from specifically designed numerical tools (Gott 1975; Williams, Babul & Dalcanton 2004) as well as full cosmological *N*-body simulations (e.g. Frenk et al. 1985; Quinn, Salmon & Zurek 1986; Efstathiou et al. 1988; Zaroubi, Naim & Hoffman 1996). One important finding along this latter line was that cold dark matter (CDM) haloes with different masses show similar scaled spherically averaged density profiles (Dubinski & Carlberg 1991; Crone, Evrard & Richstone 1994). Navarro, Frenk & White (1997) showed that they are well fitted down to about one-hundredth of the total radius by a simple analytic expression, the so-called Navarro–Frenk–White (NFW) profile, that deviates from a power law. This finding opened a lively debate about the value of the central asymptotic behaviour of the halo density profile (e.g. Fukushige & Makino 1997; Moore et al. 1998; Ghigna et al. 2000; Jing & Suto 2000; Power et al. 2003; Hayashi et al.

2004). More recently, the Einasto (1965) profile was shown to give even better fits down to smaller radii (Navarro et al. 2004, 2010; Merritt et al. 2005, 2006).

The origin of this density profile remains to be understood. Certainly, it can only arise from the way haloes aggregate their mass, which, in hierarchical cosmologies, is through continuous mergers. However, the dynamical effect of mergers depends on the relative mass of the captured and capturing haloes, $\Delta M/M$. For this reason, it is usually distinguished between minor and major mergers ($\Delta M/M$ greater or less than about 0.3; Salvador-Solé et al. 2007). Major mergers each have a dramatic effect on the structure of the object, while minor mergers contribute jointly, together with the capture of diffuse matter (if any), to the so-called accretion that yields only a small secular effect on the accreting object. Some authors (Raig et al. 1998; Syer & White 1998; Subramanian, Cen & Ostriker 2000; Dekel, Devor & Hetzroni 2003) studied the possibility that the non-power-law density profile for simulated haloes is the result of repeated major mergers. Others (Avila-Reese, Firmani & Hernández 1998; Huss, Jain & Steinmetz 1999; Del Popolo et al. 2000; Ascasibar et al. 2004; MacMillan, Widrow & Henriksen 2006) concentrated on the effects of pure accretion (PA), which proceeds according to the simple SI model above from peaks (secondary maxima) in the primordial random Gaussian density field (Doroshkevich 1970; Bardeen et al. 1986). The density profile found in this latter scenario appears to be similar, indeed, to that of simulated haloes. Furthermore, recent cosmological simulations have confirmed that major mergers play no central role in setting the structure and kinematics of dark matter haloes (Wang & White 2009). However, the reason why major mergers would not alter the density profile set by PA is not understood.

In the present paper, we develop an accurate model of halo density profile that clarifies all these issues. For simplicity, we consider pure dark matter systems, i.e. we neglect the effects of baryons on halo structure. This will allow us to directly compare the theoretical predictions of the model to the results of *N*-body simulations. This model is built within the SI framework and uses the peak formalism, which assumes there is a one-to-one mapping between haloes and the density peaks. However, peaks are not assumed to be spherically symmetric and endowed with their typical *filtered* density profile calculated by Bardeen et al. (1986, hereafter the BBKS profile) as usual, but we take into account that they are triaxial (Doroshkevich 1970; Bardeen et al. 1986) and consider their accurate spherically averaged *unconvolved* density profile. In addition, we account for the initial peculiar velocities believed to affect the central halo density profile (Hiotelis 2002; Ascasibar et al. 2004; Mikheeva, Doroshkevich & Lukash 2007). Finally, instead of making use of the usual adiabatic invariant, poorly justified near turnaround and greatly complicating the analytic derivation of the final density profile, we take advantage of the fact that accreting haloes develop outwardly, keeping their instantaneous inner structure unaltered. The validity of such an assumption, hereafter simply referred to as inside-out growth, is accurately checked by verifying that the trends observed in simulated haloes evolving by smooth accretion are reproduced by an analytic model where the haloes are forced to grow inside-out.

And what about the fact that major mergers are ignored in SI? This important caveat affects the modelling through SI not only of the halo density profile, as mentioned, but also of halo statistics in the so-called peak formalism (Peacock & Heavens 1990; Manrique & Salvador-Solé 1995, 1996, hereafter MSSa and MSSb, respectively; Bond & Myers 1996; Manrique et al. 1998) which relies on the ansatz that there is a one-to-one correspondence between

haloes and peaks as in spherical collapse,[1] although no such one-to-one correspondence is actually found in simulations (Katz, Quinn & Gelb 1993); this is because peaks show nested configurations (MSSa) which are not corrected for. If one concentrates in simply checking whether or not halo seeds, hereafter also called proto-haloes, coincide with peaks, then the answer is positive in all but a few per cent of cases compatible with the frequency of non-fully virialized haloes (Porciani, Dekel & Hoffman 2002). However, there is still the problem that, in principle, major mergers should blur the correspondence between peaks and haloes arising from SI. In the present paper, we argue that the reason why halo statistics and the spherically average density profile of virialized haloes seem to be unaffected by major mergers is that virialization is a real relaxation process. We stress that the model deals with *fully* virialized haloes. This is important because, after a major merger, the density profile of a halo spends some time to adopt a stable density profile.

The outline of the paper is as follows. In Section 2, we present some general relations holding for all systems regardless of their symmetry. Taking into account these relations, we develop in Section 3 the model for triaxial haloes grown by PA. In Section 4, we calculate the properties of typical protohaloes and use them in Section 5 to derive the typical spherically averaged density profile for CDM haloes. In Section 6, we discuss the effects of major mergers. The main results are summarized in Section 7.

Throughout the paper, we adopt the ΛCDM 7-year *Wilkinson Microwave Anisotropy Probe* (Komatsu et al. 2011) concordance model. In spite of this, we use Newtonian dynamics with null cosmological constant as its effects are irrelevant at the scale of virialized haloes. A package with the numerical codes used in the present paper is publicly available from www.am.ub.es/~cosmo/haloes&peaks.tgz.

2 GENERAL RELATIONS FOR SPHERICAL AVERAGED PROFILES

In the present section, we derive some general relations for spherically averaged quantities that hold for any arbitrary system regardless of its symmetry and that will later be used to build the model.

Consider a self-gravitating system with arbitrary mass distribution, aggregation history and dynamical state. The local density and gravitational potential can be split in the respective spherical averages around any given point and the corresponding residuals:

$$\rho(r, \theta, \varphi) = \langle \rho \rangle(r) + \delta\rho(r, \theta, \varphi), \tag{1}$$

$$\Phi(r, \theta, \varphi) = \langle \Phi \rangle(r) + \delta\Phi(r, \theta, \varphi). \tag{2}$$

The spherically averaged gravitational potential,

$$\langle \Phi \rangle(r) = \frac{1}{4\pi} \int_0^{2\pi} d\varphi \int_0^{\pi} d\theta \, \sin\theta \, \Phi(r, \theta, \varphi), \tag{3}$$

satisfies, by the Gauss theorem, the usual Poisson integral relation for spherically symmetric systems:

$$\frac{d\langle \Phi \rangle(r)}{dr} = \frac{GM(r)}{r^2}, \tag{4}$$

where $M(r)$ is the mass within r:

$$M(R) = 4\pi \int_0^R dr \, r^2 \, \langle \rho \rangle(r). \tag{5}$$

---

[1] The excursion set formalism is also based on a one-to-one correspondence between haloes and overdense regions in the initial density field as in spherical collapse.

Taking into account the null spherical averages of $\delta\rho$ and $\delta\Phi$ (see equations 1 and 2), the potential energy within the sphere of radius R,

$$W(R) = \frac{1}{2}\int_0^R dr\, r^2 \int_0^{2\pi} d\varphi \int_0^\pi d\theta\, \sin\theta\, \rho(r,\theta,\varphi)\, \Phi(r,\theta,\varphi), \quad (6)$$

can be rewritten as

$$\begin{aligned}
W(R) &= 2\pi \int_0^R dr\, r^2 [\langle\rho\rangle(r)\,\langle\Phi\rangle(r) + \langle\delta\rho\,\delta\Phi\rangle] \\
&= -4\pi \int_0^R dr\, r^2 \langle\rho\rangle(r)\, \frac{GM(r)}{r} + 2\pi \int_0^R dr\, r^2 \langle\delta\rho\,\delta\Phi\rangle \\
&\equiv \mathcal{W}(R) + \delta\mathcal{W}(R),
\end{aligned} \quad (7)$$

where we have introduced the 'spherical' potential energy within R:

$$\mathcal{W}(R) = -4\pi \int_0^R dr\, r^2 \langle\rho\rangle(r)\, \frac{GM(r)}{r}. \quad (8)$$

The second equality in equation (7) follows from partial integration of the first term on the right-hand side of the first equality, then application of the relation (4), and one new partial integration, choosing the origin of the spherically averaged potential so as to have

$$\langle\Phi\rangle(R) = -\frac{GM(R)}{R}. \quad (9)$$

Note that, for spherically symmetric systems, this boundary condition coincides with considering the usual potential origin at infinity and the system truncated at R.

The kinetic energy within R is

$$K(R) = 2\pi \int_0^R dr\, r^2 \langle\rho\rangle(r)\, \sigma^2(r), \quad (10)$$

$\sigma^2(r)$ being the velocity variance in the infinitesimal shell at r.[2] Thus, the total energy of the sphere, $E(R) = K(R) + W(R)$, takes the form

$$\begin{aligned}
E(R) &= 4\pi \int_0^R dr\, r^2 \langle\rho\rangle(r) \left[\frac{\sigma^2(r)}{2} - \frac{GM(r)}{r}\right] \\
&+ 2\pi \int_0^R dr\, r^2 \langle\delta\rho\,\delta\Phi\rangle(r) \equiv \mathcal{E}(R) + \delta\mathcal{E}(R),
\end{aligned} \quad (11)$$

where we have introduced the 'spherical' total energy

$$\mathcal{E}(R) = 4\pi \int_0^R dr\, r^2 \langle\rho\rangle(r) \left[\frac{s^2(r)}{2} - \frac{GM(r)}{r}\right]. \quad (12)$$

Note that $\mathcal{E}(R)$ is written in terms of the 'spherical' velocity variance $s^2(r)$, different, in general, from the ordinary velocity variance,

$$\sigma^2(r) = s^2(r) + \delta s^2(r), \quad (13)$$

through the residual $\delta s^2(r)$ to be specified, contributing to the residual $\delta\mathcal{E}(r)$. In other words, there is some freedom in the definition of $s^2(r)$. We will come back to this point later.

So far we have considered a system with arbitrary mass distribution (symmetry), aggregation history and dynamical state. If the system is in addition in equilibrium, then multiplying the steady collisionless Boltzmann equation (e.g. equation 4p-2 in Binney &

Tremaine 1987) by the radial particle velocity and integrating over velocity and solid angle, we are led to

$$\begin{aligned}
&\frac{d\left(\langle\rho\rangle\sigma_r^2\right)}{dr} + \frac{\langle\rho\rangle(r)}{r}\left[3\sigma_r^2(r) - \sigma^2(r)\right] \\
&= -\frac{1}{4\pi}\int_0^{2\pi} d\varphi \int_0^\pi d\theta\, \sin\theta\, \rho(r,\theta,\varphi)\, \partial_r\Phi(r,\theta,\varphi),
\end{aligned} \quad (14)$$

where ∂_r stands for radial partial derivative.[3] Taking into account equation (4), equation (14) adopts the form

$$\begin{aligned}
&\frac{d\left(\langle\rho\rangle\sigma_r^2\right)}{dr} + \frac{\langle\rho\rangle(r)}{r}\left[3\sigma_r^2(r) - \sigma^2(r)\right] \\
&= -\langle\rho\rangle(r)\frac{GM(r)}{r^2} - \langle\delta\rho\,\partial_r(\delta\Phi)\rangle(r),
\end{aligned} \quad (15)$$

identical to the Jeans equation for spherically symmetric systems in equilibrium but for the last term on the right-hand side. Multiplying equation (15) by $4\pi r^3$ and integrating over the sphere of radius R, the same steps leading to the scalar virial relation for spherically symmetric self-gravitating systems now lead to

$$\begin{aligned}
&4\pi R^3 \langle\rho\rangle(R)\sigma_r^2(R) - 2K \\
&= -4\pi \int_0^R dr\, r^2 \langle\rho\rangle(r)\frac{GM(r)}{r} - 4\pi \int_0^R dr\, r^3 \langle\delta\rho\,\partial_r\delta\Phi\rangle(r).
\end{aligned} \quad (16)$$

Therefore, defining the so-called 'spherical' radial velocity variance $s_r^2(r)$ through

$$\sigma_r^2(r) = s_r^2(r) + \delta s_r^2(r), \quad (17)$$

with

$$\delta s_r^2(r) = \frac{1}{r^3 \langle\rho\rangle(r)} \int_0^r d\tilde{r}\, \tilde{r}^2 \left[\delta s^2(\tilde{r}) - \tilde{r}\langle\delta\rho\,\partial_r\delta\Phi\rangle(\tilde{r})\right], \quad (18)$$

the virial relation (16) takes the usual form for spherically symmetric systems,

$$4\pi R^3 \langle\rho\rangle(R)\, s_r^2(R) = 4\pi \int_0^R dr\, r^2 \langle\rho\rangle(r) \left[s^2(r) - \frac{GM(r)}{r}\right], \quad (19)$$

from now on called the 'spherical' virial relation. Furthermore, defining the 'spherical' scaled surface pressure term (from now on simply spherical surface term), $\mathcal{S}(R)$, equal to the member on the left-hand side of equation (19) over the absolute value of $\mathcal{W}(\mathcal{R})$, the spherical virial relation (19) adopts the usual compact form

$$\frac{2\mathcal{E}(R)}{\mathcal{W}(R)} = 1 - \mathcal{S}(R). \quad (20)$$

As can be seen, all the ordinary quantities X can be expressed in the form $X = \mathcal{X} + \delta\mathcal{X}$, with the quantities $\mathcal{X}$ having the same form for spherically symmetric systems, hence the reason they are labelled 'spherical'. The residuals $\delta\mathcal{X}$ always measure the deviation from sphericity of the quantities X in the sense that when $\delta\rho$ and $\delta\Phi$ vanish, $\delta\mathcal{X}$ also vanish and X become equal to the spherical counterparts $\mathcal{X}$ and, hence, recover the form for spherically symmetric systems. The dimensionless quantities $|\delta\mathcal{X}/\mathcal{X}|$ are, however, not necessarily less than 1, so we should not look at the spherical quantities $\mathcal{X}$ as zeroth-order approximations of X in expansion series on small deviations from sphericity; they are fully exact quantities and so are also the relations between them. In particular, equations (5),

---

[2] Such a velocity variance coincides with the spherical average of the local value. Therefore, equation (10) could also be written in terms of the local velocity variance in angular brackets.

[3] To derive equation (14), conventional conditions such as the continuity of the local density and mean velocity and the fact that the velocity distribution function vanishes for large velocities are needed.

(12) and (20), respectively, giving the mass, spherical total energy and spherical virial relation or, equivalently, the relations

$$\langle\rho\rangle(r) = \frac{1}{4\pi r^2}\frac{dM}{dr}, \tag{21}$$

$$s^2(r) = 2\left[\frac{d\mathcal{E}/dr}{dM/dr} + \frac{GM(r)}{r}\right] \tag{22}$$

and

$$s_r^2(r) = \frac{2\mathcal{E}(r) - \mathcal{W}(r)}{r\,dM/dr} \tag{23}$$

following from their differentiation are exact and hold unchanged regardless of the particular shape of the object. Thus, the profiles $\langle\rho\rangle(r)$, $s^2(r)$ and $s_r^2(r)$ *do not depend on shape* and can be determined by solving equations (21) and (22). In contrast, the ordinary kinematic profiles $\sigma^2(r)$ and $\sigma_r^2(r)$ cannot be obtained from a similar set of equations because they depend explicitly on the shape of the object.

We want to remark that even if the spherical quantities *at any given moment* behave as their ordinary counterparts in spherically symmetric systems, the relation between their values *in different epochs* may not be the same as in such systems. For instance, the spherical total energy inside spheres of fixed mass may not be conserved in the absence of shell-crossing.[4] Only one specific choice of $s^2(r)$ will ensure such a conservation. Note also that, for any arbitrary mass distribution, it might not be possible to have only one profile $s^2(r)$ satisfying that condition for the whole series of embedded spheres the system decomposes into. However, in the case of a centred triaxial system, this is always possible, thanks to the ordered radial mapping of the mass distribution. From now on, we assume such a symmetry and the conservation of the spherical total energy in the absence of shell-crossing. This is crucial for the model as it will allow us to fix the density profile for a virialized object from the properties of its seed (see Section 3).

3 THE MODEL

We will concentrate, in a first step, on triaxial systems *evolving by PA*. This includes the case of accretion along filaments.

3.1 Inside-out growth

The model relies on the assumption that accreting objects grow inside-out. This is consistent with the properties of simulated haloes (Salvador-Solé, Solanes & Manrique 1998; Helmi, White & Springel 2003; Salvador-Solé, Manrique & Solanes 2005; Romano-Díaz et al. 2006; Wang et al. 2011). In Manrique et al. (2003) and Salvador-Solé et al. (2007), it was shown that the assumption that (spherical) haloes grow inside-out at the typical cosmological accretion rate automatically leads to a density profile à la NFW. Nonetheless, to be fully confident about it, we show below that such a growth is naturally expected and in agreement with the detailed results of simulations.

In SI, the isodensity contours in the triaxial seed expand, without crossing each other, until they reach turnaround. This expansion is achieved in linear regime with all particles moving radially,

so the axial ratios of shells are conserved. However, after reaching turnaround, particles collapse and rebound non-radially, so the shape of the isodensity contours changes. Shell-crossing causes a *secular* energy transfer between shells so that particles initially lying in a turnaround ellipsoid reach their new apocentre at a smaller radius and not simultaneously. However, the energy lost by particles in one orbit is small, so the typical time of apocentre variation is substantially greater than the typical orbital period, implying that particles belonging to one turnaround ellipsoid will still trace an effective apocentre surface, which for symmetry reasons will also be an ellipsoid although smaller in size and with different axial ratios. Repeating the same reasoning from each new apocentre ellipsoid, we have that any turnaround ellipsoid evolves through a continuous series of ellipsoidal apocentre surfaces that progressively shrink and change their shape until they stabilize.

During such an evolution, apocentre ellipsoids never cross each other. If two of them had a common point, particles belonging to the two surfaces at that point (with null velocities) would follow the same evolving orbits, so the two surfaces would always be in contact, but this is meaningless because different turnaround ellipsoids come from different isodensity contours in the seed which do not intersect. Thus, during virialization, the system contracts orderly, *without apocentre-crossing*, and when a new apocentre ellipsoid stops shrinking, it necessarily places itself beyond all previously stabilized apocentre ellipsoids. Thus, the central steady object necessarily grows from the inside out according to the gradual deposition of particles with increasingly larger apocentre surfaces.

In the above reasoning, we assumed that orbits eventually stabilize. However, new shells are constantly arriving and crossing the growing halo; consequently, orbits only approximately stabilize. It is therefore worthwhile verifying the validity of this approximation. This can be accurately checked by means of the detailed follow-up of the density profile for CDM haloes in simulations. Zhao et al. (2009) and Muñoz-Cuartas et al. (2011) carried out such a follow-up and found that the r_s and M_s NFW shape parameters[5] of accreting haloes are not constant but vary slightly with time. This was interpreted as evidence that the inner structure of accreting haloes is changing. However, this is not the only possible interpretation. As the density profile of haloes *is not perfectly fitted* by the NFW profile,[6] even if the inner density profile did not change, its fit by the NFW law out to progressively larger radii should result in slightly different best values of r_s and M_s.

To confirm that our interpretation for this change is correct, we have followed in the M_s–r_s log–log plane the evolution of accreting haloes forced to grow *inside-out* at the typical accretion rate given by the excursion set formalism according to Salvador-Solé et al. (2007) model. The result, in the same cosmology as used in Zhao et al. (2009), is shown in Fig. 1. Even if, by construction, haloes grow inside-out without changing their instantaneous inner structure, when their density profile is fitted by an NFW profile, they are found to move in the M_s–r_s log–log plane along one fixed direction over a distance that increases with current halo mass. This behaviour is *identical* to that found by Zhao et al.: accreting haloes moved in the M_s–r_s log–log plane along straight lines with exactly the same universal slope ($M_s \propto r_s^{1.65}$) as in our experiment and ended up at $z = 0$ lying along another straight line, with a different

---

[4] If one chooses $s^2(r) \equiv \sigma^2(r)$, the spherical total energy is not conserved in ellipsoidal systems because any given sphere exchanges energy with the rest of the system.

[5] M_s is defined as the mass within the scale radius r_s where the logarithmic slope of the density profile is equal to -2.

[6] The larger the mass, the closer the density profile is to a power law with index ~ -1.5–2 (Tasitsiomi et al. 2004).
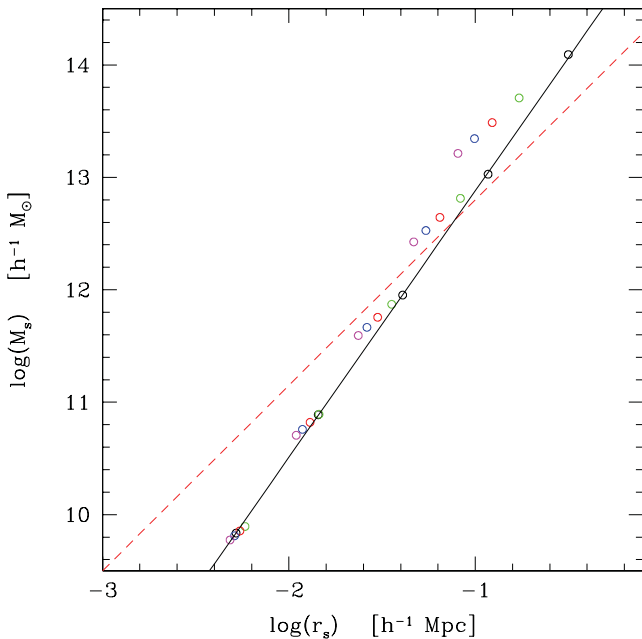
Figure 1. Tracks followed in the M_s–r_s plane by typical accreting haloes developing inside-out, with current masses, M, equal to 10^{11}, 10^{12}, 10^{13}, 10^{14} and 10^{15} M$_\odot$ (from bottom to top) at $z = 0, 2, 4, 6$ and 8 (circles essentially from right to left, respectively, in black, green, red, blue and magenta). The straight dashed red line shows the universal direction followed by such tracks, identical to that found by Zhao et al. (2009) in full cosmological simulations. The black straight line shows the M_s–r_s relation obtained at $z = 0$ also identical to that found in Zhao et al. (2009; see fig. 22).

slope ($M_s \propto r_s^{2.48}$) also identical to that found in our experiment (see their fig. 22). The fact that our constrained model reproduces the observed trend convincingly demonstrates haloes primarily grow inside-out.

3.2 Radius encompassing a given mass

As we will show, by assuming that haloes grow inside-out via PA and that the spherical total energy in spheres of fixed mass is conserved in the absence of shell-crossing, we are able to infer the radius enclosing a given mass in a halo from the spherical energy distribution of its progenitor protohalo.

To do this, we will consider the virial relation (20) for a perfectly uniform sphere with mass M, which implies $\mathcal{W}(M) = -3GM^2/(5R)$, with spherical total energy $\mathcal{E}(M)$ equal to that of the system at turnaround $\mathcal{E}_{ta}(M)$ and null spherical surface term $\mathcal{S}(M)$:

$$R(M) = -\frac{3}{10}\frac{GM^2}{\mathcal{E}_{ta}(M)}. \tag{24}$$

This equation is the often used estimate for the radius encompassing mass M in spherical systems with an unknown internal mass distribution (Bryan & Norman 1998). In principle, $R(M)$ is not believed to give an exact measure of that mass in the real virialized object as this has non-uniform density profile, its spherical total energy is equal to $\mathcal{E}(M)$ instead of $\mathcal{E}_{ta}(M)$ and its surface term is not null. Yet, as shown below, as a consequence of *the inside-out growth of accreting objects formed by PA*, the inaccuracies above exactly cancel and both radii turn out to fully coincide.

To see this, we will deform the system since its shells reach turnaround so as to construct a virialized toy object satisfying the conditions leading to equation (24). This is only possible in PA

where the equivalent radius of turnaround ellipsoids increases with increasing time and the central virialized object grows inside-out. Shells reaching turnaround can then be *virtually* contracted one after the other without any crossing so as to match the mass profile $M(r)$ (although not necessarily the ellipsoidal isodensity contours) of the real virialized object developed until some time t. By 'virtual' motion we mean a motion of shells that preserves their particle energy and angular momentum, but is disconnected from the real timing of the system. Of course, such a motion will not recover at the same time the axial ratios of the isodensity contours of the virialized object, but we only need to recover the mass profile, which by conveniently contracting each new shell is guaranteed (there is one degree of freedom: the final equivalent radius of the contracted ellipsoidal shell, and one quantity to match: the mass within the new infinitesimally larger radius). By construction, the new toy object so built has the same mass profile $M(r)$ [although not the total energy profile $E(r)$ due to the different ellipsoidal mass distribution] as the virialized object. However, the spherical total energy in such a toy object is equal to that at turnaround, $\mathcal{E}_{ta}[M(r)]$, as there has been no shell-crossing and $\mathcal{E}$ is conserved for the appropriate choice of $s^2(r)$ (see Section 2).

Of course, such a toy object is not in equilibrium. However, the quantity $\mathcal{E}_{ta}(R) - \widetilde{\mathcal{W}}(R)$, with $\widetilde{\mathcal{W}}(R)$ equal to the potential energy of a homogeneous sphere with mass M, is positive (see equation 25 below). Therefore, we can virtually expand each ellipsoidal isodensity contour of the toy object, from the centre out to the edge avoiding shell-crossing, so as to end up with a uniform density equal to the mean density $\bar{\rho}(R)$ of the real object inside R and still have an excess of spherical kinetic energy. Thus, this can be redistributed over the sphere and the radial and tangential components of the spherical velocity variance, $\widetilde{s}(r)$, can be locally exchanged so as to satisfy the spherical virial relation (19) at every radius. This is again possible to achieve because there are two degrees of freedom, $\widetilde{s}(r)$ and $\widetilde{s}_r(r)$, and two conditions to fulfil, the spherical total kinetic energy in excess and the spherical virial equation. In this way, we have built a steady homogeneous toy object with radius, mass and total energy, respectively, equal to R, M and $\mathcal{E}_{ta}(M)$ and with null value of $\widetilde{s}_r(R)$ (there is no density outside the sphere because shells having not reached turnaround at t have not been contracted). Hence, this uniform toy object satisfies the spherical virial relation

$$\frac{2\mathcal{E}_{ta}(R)}{\widetilde{\mathcal{W}}(R)} = 1, \tag{25}$$

which, given the equality $\widetilde{\mathcal{W}}(R) = -3GM^2/(5R)$, implies equation (24).

The exact equation (24) allows one to determine the spherically averaged density profile of the virialized object from the properties of its seed. To do this, we must simply take into account that, during the initial expanding phase of shells, there is no shell-crossing, so the spherical total energy in spheres with fixed mass is conserved. We can then replace, in equation (24), $\mathcal{E}_{ta}(M)$ by its value in the protohalo, $\mathcal{E}_p(M)$, and obtain, by inversion of $r(M)$, the mass profile $M(r)$ and, through equation (21), the spherically averaged density profile $\langle\rho\rangle(r)$ of the virialized object from the spherical total energy distribution in the seed.

Furthermore, as the functions $\langle\rho\rangle(r)$, $s^2(r)$ and $s_r^2(r)$ do not depend on the shape of the object, we can think in the spherically symmetric case to infer the latter two functions from the former one. In such objects, orbits are purely radial because they collapse and virialize radially. We therefore have $s^2(r) = s_r^2(r)$. Equations (22) and (23) then lead to a differential equation for $\mathcal{E}(r)$ that can be readily integrated for the boundary condition $\mathcal{E} = 0$ at $r = 0$, the result

being

$$\mathcal{E}(R) = -R \int_0^R dr \left[4\pi \langle \rho \rangle(r)\, GM(r) + \frac{\mathcal{W}(r)}{2r^2} \right].$$ (26)

Once $\langle \rho \rangle(r)$ is known, we can calculate $\mathcal{W}(r)$ (equation 6) and then $\mathcal{E}(R)$ (equation 26), and apply any of the two relations (22) and (23) to infer the profile $s^2(r)$. However, the interest of this expression is only formal because, as mentioned, the profile $s^2(r)$ is not observable, not even in the spherically symmetric case where $s(r) = \sigma(r)$ and $s_r(r) = \sigma_r(r)$. The reason for this is that objects formed by PA are never spherically symmetric. The tidal field of surrounding density fluctuations causes spherically symmetric seeds to undergo ellipsoidal collapse (Zeldovich 1970). Even if such a tidal field is artificially removed, the system suffers radial orbit instability, also leading to triaxial virialized objects (Huss et al. 1999; MacMillan et al. 2006).

The expression (26) is nonetheless useful to compute the spherical total energy dissipation factor since the time of the protohalo, $\mathcal{D}(M) \equiv \mathcal{E}(M)/\mathcal{E}_p(M)$, with $\mathcal{E}_p(M)$ given by equation (24). This has the following interesting implication. In objects formed by PA, there is always some spherical energy loss through shell-crossing during virialization, so $\mathcal{D}(M)$ is greater than 1. Taking into account equations (20) and (25), this dissipation factor can be written in the form

$$\mathcal{D}(M) = \frac{\mathcal{W}(M)}{\widetilde{\mathcal{W}}(M)} \left[1 - \mathcal{S}(M) \right].$$ (27)

Thus, if $\mathcal{D}(M)$ is greater than 1, the ratio

$$\frac{\mathcal{W}(M)}{\widetilde{\mathcal{W}}(M)} = \frac{5}{6} \left[1 + \int_0^{R(M)} \frac{dr}{R(M)} \frac{r^4 \, \bar{\rho}^2(r)}{R^4 \, \bar{\rho}^2(R)} \right]$$ (28)

must also be greater than 1.[7] By differentiation and after a little algebra, it can be seen that the ratio $\mathcal{W}(M)/\widetilde{\mathcal{W}}(M)$ is greater than 1 provided only $\bar{\rho}(r)$ is outward-decreasing. Consequently, we are led to the conclusion that the spherically averaged mean inner density profile of any collisionless dissipationless virialized object formed hierarchically (through PA but also through major mergers; see Section 6) *is necessarily outward-decreasing*.

4 PROTOHALOES

According to the previous results, to calculate the spherically averaged density profile for a CDM halo grown by PA we only need the spherical energy distribution, $\mathcal{E}_{ta}(M)$, of its seed, namely a peak in the initial density field filtered at the mass scale of the halo. The cosmic time t_i where the initial density field has to be considered is arbitrary although small enough for the protohalo to be in linear regime.

Such a spherical energy distribution is given, in the parametric form, by the spherical total energy of the protohalo,

$$\mathcal{E}_p(R_p) = 4\pi \int_0^{R_p} dr_p\, r_p^2\, \langle \rho_p \rangle(r_p)$$

$$\times \left\{ \frac{[H_i r_p - v_p(r_p)]^2}{2} + \frac{\sigma_p^2(R_p)}{2} - \frac{GM(r_p)}{r_p} \right\},$$ (29)

in centred spheres of radii R_p encompassing the masses M,

$$M(R_p) = 4\pi \int_0^{R_p} dr_p\, r_p^2\, \langle \rho_p \rangle(r_p).$$ (30)

In equations (29) and (30), H_i is the Hubble constant at the cosmic time t_i of the protohalo, $\langle \rho_p \rangle(r_p)$ is its spherically averaged density profile, $v_p(r_p)$ is the peculiar velocity, to zeroth order in the deviations from sphericity, due to the gravitational pull by the mass excess within the radius r_p and $\sigma_p(R_p)$ is the uniform and isotropic background peculiar velocity dispersion inside the sphere of radius R_p.[8]

The peculiar velocity $v_p(r_p)$ is (e.g. Peebles 1980)

$$v_p(r_p) = \frac{2G \left[M(r_p) - 4\pi r_p^3 \rho_i/3 \right]}{3H_i r_p^2},$$ (31)

ρ_i being the mean cosmic density at t_i.[9] Bringing this expression of $v_p(r_p)$ into equation (29) and neglecting the second-order term in the perturbation with $v_p^2(r_p)$ [the term with $\sigma^2(R_p)$ may be greater than this owing to the contribution of $\sigma_{DM}^2(t_i)$], we are led to

$$\mathcal{E}_p(R_p) = \frac{5}{3} \mathcal{E}_p^H(R_p) + M(R_p) \frac{\sigma_p^2(R_p)}{2},$$ (32)

where $\mathcal{E}_p^H(R_p)$ stands for the spherical total energy of the protohalo in the case of pure Hubble flow (i.e. equation 29 with null v_p and σ_p). In principle, $\sigma_p^2(R_p)$ has two contributions: one arising from the dark matter particle velocities at decoupling, adiabatically evolved until the time t_i, $\sigma_{DM}^2(t_i)$, and another one caused by random density fluctuations. Following the exact prescription by Mikheeva et al. (2007) for this latter contribution, we arrive at

$$\sigma_p^2(R_p) = \sigma_{DM}^2(t_i) + \Sigma_i^2 \int_0^\infty \frac{dk}{2\pi^2} P(k) \left[1 - e^{-k^2 R_p^2} \right]^2$$

$$= \sigma_{DM}^2(t_i) + \Sigma_i^2 \left[\sigma_{-1}^2(0) - 2\sigma_{-1}^2(R_p) + \sigma_{-1}^2(\sqrt{2}R_p) \right],$$ (33)

where Σ_i is defined as $\sqrt{2}\pi H a_i^2$, a_i being the initial cosmic scale factor,[10] and $\sigma_{-1}^2(R_f)$ is the spectral moment of order -1 for the power spectrum, $P(k)$, with the jth-order moment given by

$$\sigma_j^2(R_f) = \int_0^\infty \frac{dk}{2\pi^2} P(k)\, k^{2j+2}\, e^{-k^2 R_f^2}.$$ (34)

However, the velocity variance due to random density fluctuations, $\sigma_p^2(R_p) - \sigma_{DM}^2(t_i)$ (see equation 33), turns out to be several orders of magnitude less than $GM(R_p)/R_p$ (a factor of $\sim 10^{-6}$ in the concordance model adopted here). Consequently, it can be neglected in $\mathcal{E}_p(M)$ (equation 29), contrary to the claims made by Hiotelis (2002), Ascasibar et al. (2004) and Mikheeva et al. (2007) that such a velocity dispersion may affect the central density profile for CDM haloes. The former two authors reached this conclusion by analysing the effects of velocity dispersions that, unlike those used here, were not consistently inferred from the random density fluctuations. Mikheeva et al. used the same derivations for the dispersion as used here; however, they considered the fluctuations within the whole protohalo, whereas we account for random density fluctuations within each sphere of radius R_p. In including fluctuations from the whole protohalo, Mikheeva et al. included velocities induced by *external* density fluctuations with masses possibly larger than the own mass of the sphere. This overestimates the velocity dispersion in the sphere because external density fluctuations cause a bulk velocity, not a velocity dispersion. And the bulk velocity of a sphere

---

[7] As $\mathcal{W}(M)/\widetilde{\mathcal{W}}(M)$ is positive (see equation 28), the factor $1 - \mathcal{S}(M)$ must also be positive and less than 1.

[8] The starting value of the spherical total energy can be computed taking $s_p^2 \equiv \sigma_p^2$.

[9] In equation (31), we have taken into account that the cosmic virial factor $f(\Omega) \approx \Omega^{0.1}$ is at t_i, very approximately equal to 1.

[10] At small t_i, this is very approximately equal to the cosmic growth factor.

does not hamper its collapse, whereas the internal velocity dispersion does, as found by Mikheeva et al. for small enough R_p. The only velocity dispersion that does not diminish with decreasing R_p and, hence, can really set a minimum halo mass is that intrinsic to dark matter particles, $\sigma_{DM}^2(t_i)$. However, this is negligible in CDM cosmologies.

And what about the spherically averaged peak density profile, $\langle \rho_p \rangle (r_p)$? The BBKS profile calculated by Bardeen et al. (1986) gives the typical (average) spherically averaged density contrast profile for peaks *filtered* with a Gaussian window. Unfortunately, the convolution by a Gaussian window results in some information loss, so the BBKS profile cannot be used to infer the desired profile. In addition, the *average* profile of purely accreting haloes with M at t may not coincide with the profile arising from the *average* profile of the corresponding seeds. However, we can still find the typical (in the sense below) spherically averaged density profile of protohaloes.

Since in PA haloes grow inside-out, the density profile inside every inner ellipsoid exactly matches that of one halo ancestor, also evolved by PA from a peak with its own density contrast and scale. Hence, the typical (average) spherically averaged density profile for purely accreting haloes with M at t must arise from a protohalo whose spherically averaged density contrast profile, $\langle \delta_p \rangle (r_p)$, convolved with a Gaussian window of radius R_f corresponding to the mass of any halo ancestor yields, at $r_p = 0$, the density contrast $\delta_{pk}(R_f)$ of the peak evolving into that ancestor:

$$\delta_{pk}(R_f) = \frac{2^{1/2}}{\pi^{1/2} R_f^{-3}} \int_0^\infty dr_p \, r_p^2 \langle \delta_p \rangle (r_p) \exp\left[-\frac{1}{2}\left(\frac{r_p}{R_f}\right)^2\right]. \quad (35)$$

According to the peak formalism (see Section 6), the typical (most probable) trajectory $\delta_{pk}(R_f)$ of peaks evolving into the series of halo ancestors ending in a halo with M at t is the solution of the differential equation (MSSb)

$$\frac{d\delta_{pk}}{dR_f} = -x_e(\delta_{pk}, R_f) \sigma_2(R_f) R_f, \quad (36)$$

with the boundary condition defined by the halo, i.e. satisfying the relations

$$\delta_{pk}(t) = \delta_c(t) \frac{G(t_i)}{G(t)} \quad (37)$$

and

$$R_f(M) = \frac{1}{q}\left[\frac{3M}{4\pi\rho_i}\right]^{1/3}, \quad (38)$$

where $G(t)$ is the cosmic growth factor, $q = 2.75$ is the radius, in units of R_f, of the collapsing cloud with volume equal to M/ρ_i, $\delta_c[t(z)] = 1.93 + (5.92 - 0.472z + 0.0546z^2)/(1 + 0.000568z^3)$ is the critical linearly extrapolated density contrast for halo formation at the redshift z (see Section 4 for those values of q and $\delta_c[t(z)]$). In equation (36), $x_e(\delta_{pk}, R_f)$ is the inverse of the average inverse curvature x (equal to minus the Laplacian over σ_2) for the distribution of curvatures (BBKS),

$$\left\langle \frac{1}{x} \right\rangle (R_f, \delta_{pk}) = \frac{(2\pi)^{-1/2}}{(1-\gamma^2)^{1/2}} \int_0^\infty dx \, \frac{1}{x} f(x) \, e^{-\frac{(x-x_\star)^2}{2(1-\gamma^2)}}, \quad (39)$$

at peaks with δ_{pk} and R_f being

$$f(x) = \frac{x^3 - 3x}{2}\left\{\mathrm{erf}\left[\left(\frac{5}{2}\right)^{1/2} x\right] + \mathrm{erf}\left[\left(\frac{5}{2}\right)^{1/2}\frac{x}{2}\right]\right\}$$
$$+ \left(\frac{2}{5\pi}\right)^{1/2}\left[\left(\frac{31x^2}{4} + \frac{8}{5}\right) e^{-5x^2/8} + \left(\frac{x^2}{2} - \frac{8}{5}\right) e^{-5x^2/2}\right], \quad (40)$$
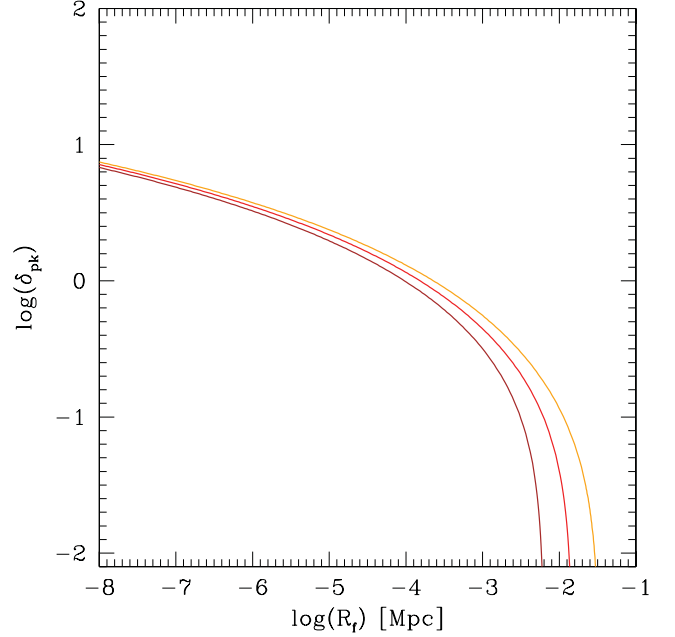
Figure 2. Typical δ_{pk}–R_f (in physical units) peak trajectory of peaks at $z = 100$ (solid lines) giving rise to the series of halo ancestors evolving by PA into haloes with current masses M equal to 10, 1 and 0.1 times the critical mass for collapse, $M_* = 3.6 \times 10^{12}$ M$_\odot$ (curves from top to bottom, respectively, in orange, red and brown).

and $\sigma_2(R_f)$ the second-order spectral moment, where γ and $x_\star$ are, respectively, defined, in terms of the spectral moments, as $\sigma_1^2/(\sigma_0\sigma_2)$ and $\gamma\delta_{pk}/\sigma_0$. This distribution function is a very peaked, quite symmetric, bell-shaped function so that the function $R_f(\delta_{pk})$, inverse of the $\delta_{pk}(R_f)$ solution of equation (36), is traced by peaks with the average (essentially equal to the most probable) inverse curvature at each point (δ_{pk}, R_f). Note that the slope $dR_f/d\delta_{pk}$ translates into the typical (average or most probable) accretion rate, dM/dt, of haloes with $M(R_f)$ at $t(\delta_{pk})$ evolving from those peaks. In Fig. 2, we show the typical peak trajectories at $z = 100$ leading to typical haloes with current masses equal to $10^{-1}M_*$, M_* and $10M_*$, where M_* is the critical mass for collapse in the concordance model (3.6×10^{12} M$_\odot$).

Given a typical peak trajectory, $\delta_{pk}(R_f)$, equation (35) is a Fredholm integral equation of first kind for $\langle \delta_p \rangle (r_p)$. Through the changes $y = r_p^2$ and $x = 1/(2R_f^2)$, it takes the form of a two-sided Laplace integral transform,

$$g(x) = \int_{-\infty}^\infty dy \, f(y) \, e^{-xy}, \quad (41)$$

with $f(y)$ and $g(x)$, respectively, equal to $y^{1/2}\langle\delta_p\rangle(y^{1/2})$ and $2\sqrt{2\pi}(2x)^{-3/2}\delta_{pk}[(2x)^{-1/2}]$, which can be solved in the standard way. Extending x to the complex space and taking $x = i2\pi\xi$, equation (41) adopts the form of a Fourier transform,

$$g(\xi) = \int_{-\infty}^\infty dy \, f(y) \, e^{-i2\pi\xi y}, \quad (42)$$

where $g(\xi) = 2\sqrt{2\pi}(i4\pi\xi)^{-3/2}[\delta_R(\xi) + i\delta_I(\xi)]$, where $\delta_R(\xi)$ and $\delta_I(\xi)$ stand, respectively, for the real and imaginary parts of $\delta_{pk}(\xi) \equiv \delta_{pk}[(4\pi\xi)^{-1/2}]$. Thus, equation (35) can be inverted by simply taking the inverse Fourier transform of equation (42).

As $f(y)$ is a real function, the real and imaginary parts of $g(\xi)$ must be even and odd, respectively. Both conditions must be satisfied at the same time, so there are only two possibilities: either
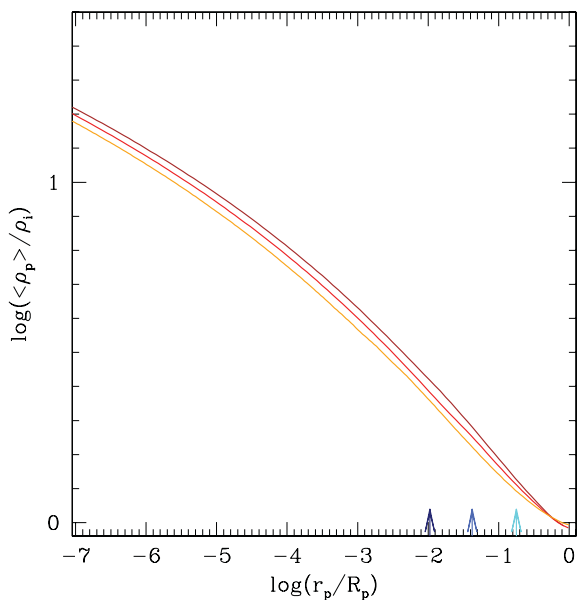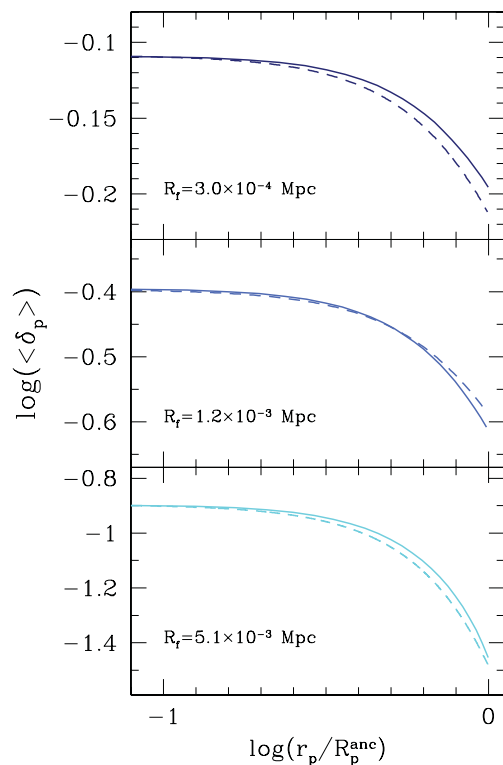
Figure 3. Spherically averaged unconvolved density profiles for the seeds of typical purely accreting haloes with the same current masses M as in Fig. 2 (same colours, now ordered from bottom to top), obtained by inversion of the peak trajectories shown in that figure. R_p is the radius of the proto-object with mass M. The filtering radii R_f/R_p used in the convolutions shown in Fig. 4 are marked with arrows.

$\delta_R(\xi) = \delta_I(\xi)$ or $\delta_R(\xi) = -\delta_I(\xi)$. The latter possibility leads to a non-physical solution, so $g(\xi)$ must be a pure imaginary odd function, i.e. $\delta_R(\xi) = \delta_I(\xi)$. To determine $\delta_{pk}(\xi)$, we must solve the differential equation (36) in the complex space for ξ, i.e. for its real and imaginary parts separately. However, as the two solutions δ_R and δ_I are identical, we can directly solve it in the real space for R_f and then take $\delta_R = \delta_I = \delta_{pk}/\sqrt{2}$, after the conversion from R_f to ξ. Once the solution $\delta_{pk}(\xi)$ is known, we can readily calculate the function $g(\xi)$ and take its inverse Fourier transform, which leads to the wanted protohalo density contrast profile, $\langle \delta_p \rangle(r_p)$, after the change $r_p^2 = y$.

The spherically averaged unconvolved protohalo density profiles, $\langle \rho_p \rangle(r_p)$, obtained from the typical peak trajectories depicted in Fig. 2 are shown in Fig. 3. In Fig. 4, we plot the convolved density contrast profiles for the seeds of three arbitrary ancestors [with masses $M(R_f)$ given by equation (38) for the three arbitrary filtering radii] of the halo with final mass M_*, corresponding to the filtering radii in units of the protohalo radius, R_f/R_p, marked with arrows in Fig. 3. For comparison, we also plot the BBKS profiles for peaks with identical central density contrasts and filtering radii. As can be seen, each couple of curves is very similar; the small deviation observed (of less than 10 per cent within the radius R_p^{anc} of each ancestor seed) is likely due to round-off errors.[11] Thus, there is no evidence that the peak leading to an object with the average spherically averaged density profile for haloes with M at t is significantly different from the average peak leading to such haloes.

Interestingly, the peak trajectories converge to a finite value (null asymptotic slope) as R_f approaches to zero, as can be seen after

---

[11] The convolution is achieved by taking the product of the 3D Fourier transform of the unconvolved density contrast profile and the Gaussian window. As the Fourier transform of the unconvolved density contrast profile has no compact support, some aliasing is present.

Figure 4. Spherically averaged density contrast profiles for the seed at $z = 100$ of a halo with current mass equal to M_* (in red in Figs 2 and 3) convolved by a Gaussian window (solid lines) with the filtering radii quoted (in physical units) and marked with arrows in Fig. 3 (same colours), compared to the BBKS profiles with identical central density contrasts and filtering scales (dashed coloured lines). R_p^{anc} are the radii of the seeds of the corresponding halo ancestors.

some algebra from the null asymptotic limit of the right-hand side member of equation (35). This in turn implies, from equation (35) and the relation between $\langle \delta \rho_p \rangle(r_p)$ and $\langle \rho_p \rangle(r_p)$, that the unconvolved density profiles for protohaloes with different masses also converge to a finite value. This is consistent with the behaviour at small radii of the unconvolved density profiles of protohaloes shown in Fig. 3. This finite limit is approached slightly more rapidly than in the case of typical peak trajectories.

5 HALO DENSITY PROFILE

Thus, to derive the typical spherically averaged density profile of a halo with M at t, we must follow the following steps: (i) solve equation (36) for the typical peak trajectory $\delta_{pk}(R_f)$ leading by PA to the typical halo with M at t; (ii) from such a peak trajectory, invert equation (35) to find $\langle \delta_p \rangle(r_p)$ and from it the spherically averaged density profile of the protohalo, $\langle \rho_p \rangle(r_p)$; (iii) given the protohalo density profile, determine the spherical energy distribution $\mathcal{E}_p(M)$ in the protohalo by means of equations (30) and (29) and (iv) making use of this latter function, invert equation (24) to find the typical mass profile $M(r)$ of the halo and, from it (equation 21), the typical spherically averaged density profile $\langle \rho \rangle(r)$.

The density profiles so obtained (hereafter the theoretical profiles) for haloes with the same masses as in Figs 2 and 3 are compared in Fig. 5 to the corresponding NFW profiles with Zhao et al. (2009) mass–concentration relation and a total halo radius equal to the virial radius R_{vir} of Bryan & Norman (1998) (essentially equal to r_{90}). As can be seen, there is good agreement between each couple of
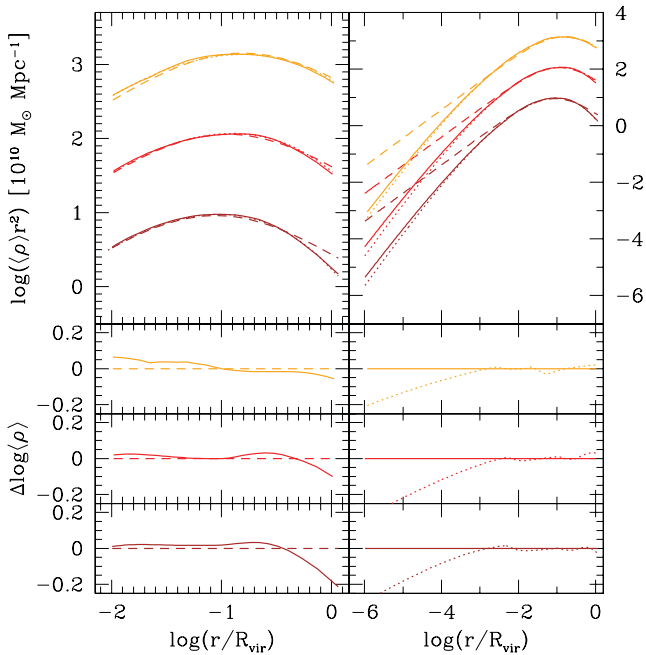
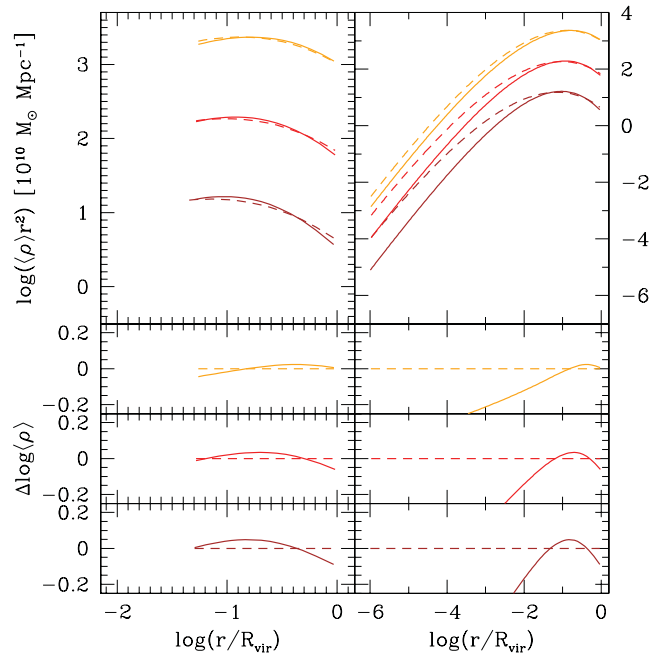**Figure 5.** Spherically averaged density profiles predicted by the present model (solid lines) for the same current masses M at $R_{\rm vir}$ as in Figs 2 and 3 (same colours, ordered as in Fig. 2), compared to the density profiles of the NFW form (dashed lines) with Zhao et al. (2009) concentrations fitting the average density profile of simulated haloes, both in the radial range covered by those authors (left) and down to a radius four orders of magnitude less (right). For comparison, we also plot the fits to the predicted density profiles by an Einasto law (dotted lines). To avoid crowding, the curves for 10 and $0.1\,M_*$ have been, respectively, shifted upwards and downwards by a factor of 3. The lower panels show the residuals of the theoretical curves from the NFW profiles (left) and of the Einasto profiles from the theoretical curves (right) for the three halo masses (same order from top to bottom).

Figure 6. Same as Fig. 5 (including colours and order) but for the comparison with the density profiles of the Einasto form (dashed lines) with Gao et al. (2008) mass-dependent parameters fitting the average density profile of simulated haloes in the ΛCDM cosmology adopted by those authors, both in the radial range covered by Gao et al., although extended out to $R_{\rm vir} \approx r_{90}$ (left) and down to the same small radii as in the right-hand panel of Fig. 5 (right). The curves for 10 and $0.1\,M_*$ have been shifted as in Fig. 5. The lower panels show the residuals (same lines) for the three halo masses (same order from top to bottom).

curves down to about one-hundredth $R_{\rm vir}$. The residuals $\Delta \log(\langle \rho \rangle)$ (prediction minus NFW profile) start being positive at $0.01R_{\rm vir}$, tend to diminish at intermediate radii (reaching slightly negative values for M_*), then increase again at moderately large radii (except for $10\,M_*$) and finally become negative near the halo edge. All these trends coincide with those shown by the same residuals (simulated halo minus NFW profile) for individual haloes in the simulations by Navarro et al. (2004; fig. 1, left-hand panels) except for the fact that the residuals of simulated haloes are notably larger, as expected (the theoretical profiles are supposed to correspond to average profiles). The only significant difference is near the halo edge, where the residuals of the theoretical profiles for low halo masses keep on decreasing for a longer radial range (see also Fig. 7). This could be due to the different halo radius used in both works: the radius adopted in the present version of the model, arising from the fit to the halo mass function predicted in the excursion set formalism (see Section 6), is likely closer to $R_{\rm vir} \approx r_{90}$ as in Zhao et al. (2009) than to r_{200} as in Navarro et al. (2004).

However, at small r, the theoretical profiles become progressively shallower and increasingly deviate from the NFW form (with constant inner logarithmic slope equal to -1). This behaviour is also in agreement with the results of numerical simulations showing that the Einasto profile gives a slightly better fit to the spherically averaged density profile for simulated haloes down to radii of about $0.001R_{\rm vir}$. In Fig. 5, we plot the Einasto profiles that better fit the theoretical profiles down to $0.01R_{\rm vir}$. As can be seen, these Einasto

profiles are still reasonably close to the theoretical profiles at radii four orders of magnitude less ($r \sim 10^{-6}R_{\rm vir}$).

In Fig. 6, the theoretical density profiles are also compared to the Einasto profiles with mass-dependent parameters according to Gao et al. (2008) and the same cosmology used by these authors (the mass-dependent Einasto parameters are not known for other cosmologies). Although Gao et al. fitted the density profile of simulated haloes only down to 0.05 the total radius,[12] the agreement between each couple of curves is similarly good as for the NFW profiles. In this case, the agreement of the theoretical profiles with the Einasto profiles at very small radii is not so good (although still much better than with the NFW profiles). However, this is likely due to the rather limited radial range covered in Gao et al.'s study. As the NFW profile gives, down to $\sim 0.01R_{\rm vir}$, similarly good fits as the Einasto profile to the density profile of simulated haloes, the results shown in Fig. 5 strongly suggest that the Einasto profile can do much better at small radii if Einasto parameters are adjusted by covering a wider radial range.

Given a protohalo with inner asymptotic density profile $\rho \propto r_{\rm p}^\alpha$, so that $M(r_{\rm p}) \propto r_{\rm p}^{(3+\alpha)}$ and $\mathcal{E}_{\rm p}(r_{\rm p}) \propto r_{\rm p}^{(5+\alpha)}$, we have, from equation (24), that $\langle \rho \rangle(r) \propto r^\alpha$. Since the protohalo has a null logarithmic slope α (see Section 4), it follows that the density profile for haloes must also have null inner logarithmic slope. In other words, there is strictly no cusp in the spherically averaged density profile for CDM haloes according to the present model.

---

[12] Gao et al. (2008) used r_{200}. To transform to the same radius $R_{\rm vir}$ as in Fig. 5, their Einasto profiles have been extended to r_{90} where we have computed the halo mass.

However, the finite central value is approached very slowly, in fact slightly more slowly than the Einasto profile (see Fig. 5).

The main differences between the density profiles predicted by the present model and by Del Popolo et al. (2000) and Ascasibar et al. (2004) models, both of which also use the SI framework, are that we do not assume spherical seeds with convolved BBKS profiles and we make use of inside-out growth instead of an adiabatic invariant to determine $\langle\rho\rangle(r)$. The model presented here is essentially equivalent to the Salvador-Solé et al. (2007) model. The key difference is that Salvador-Solé et al. (2007) used the typical cosmological accretion rate on to haloes, whereas here we explicitly make use of the typical density profile of halo seeds. However, the typical halo mass accretion rate arises, as mentioned, from the typical protohalo density profile, so this difference is just a matter of presentation, motivated by the distinct theoretical framework of the two models: the peak and the excursion set formalisms. The only formal difference between the two models, apart from the fact that Salvador-Solé et al. also assumed spherical symmetry, is that the radius encompassing a given mass adopted by these authors was inferred from equation (24) although not using the spherical total energy of the real proto-object but of its *top-hat approximation* according to Bryan & Norman (1998) prescription. This should introduce additional numerical differences between the density profiles predicted by the two models. It is also important to mention that the models by Del Popolo et al. (2000) and Ascasibar et al. (2004) and Salvador-Solé et al. (2007) include free parameters to be adjusted (the density contrast and filtering radius of the peak in the two former cases, and the value of $\Delta M/M$ setting the frontier between minor and major mergers in the latter), while the present model includes no free parameter at all.

In Fig. 7, the spherically averaged halo density profile predicted by the present model is compared to those predicted by the Del
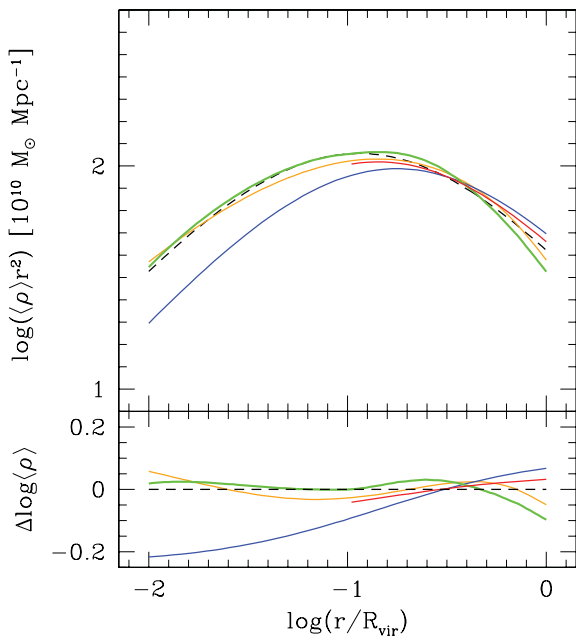
Figure 7. Spherically averaged density profile for a halo with current total mass inside $R_{\rm vir}$ equal to M_* predicted by the present model (green line), Salvador-Solé et al. (2007) model (orange line), the Ascasibar et al. (2004) model (red line) and the Del Popolo et al. (2000) model (blue line), respectively, ordered from bottom to top at the right end of each panel. The Ascasibar et al. profile is only shown at radii larger than $0.1R_{\rm vir}$ as recovered by those authors.

Popolo et al. (2000), Ascasibar et al. (2004) and Salvador-Solé et al. (2007) models, all of them in the concordance model here considered. As expected, the theoretical profile predicted by the present model is quite similar to that predicted by Salvador-Solé et al.'s model, while these two profiles substantially deviate from those predicted by the remaining models. On the other hand, the two former profiles are in better agreement with the NFW profile with Zhao et al. (2009) mass–concentration relation. Moreover, the theoretical profile derived here is the one in best agreement with such an NFW profile, which is remarkable because it is also the only theoretical profile with no free parameter to be adjusted.

6 IMPLICATIONS FOR MAJOR MERGERS

The present model has been built for haloes formed by PA. This kind of halo formation is crucial not only for the inside-out growth condition, but also for the possibility to apply the peak formalism in order to derive the peak trajectory leading to a typical halo with a given mass at a given time. The peak formalism itself is based on the existence of a one-to-one correspondence between haloes and peaks inspired in the SI model that ignores major mergers. This therefore raises two important questions. How do major mergers affect the typical spherically averaged density profile for haloes derived under these conditions? And how do they affect the peak formalism?

As shown in Section 3, given a seed with known spherically averaged density profile, we can find the spherically averaged density profile of the virialized halo evolving from it by PA, but the converse is also true. Given a halo grown by PA, we can calculate from its mass profile $M(r)$ the spherical total energy of the protohalo, $\mathcal{E}_{\rm p}(M)$ (equation 24), and then determine its spherically averaged density profile, $\langle\rho_{\rm p}\rangle(r)$, from equations (29) and (30). Therefore, there is in PA *a one-to-one correspondence between the initial and final spherically averaged density profiles*. This is a well-known characteristic of *spherical* SI (Del Popolo et al. 2000), extended in the present paper to non-spherical SI.

Interestingly, the reconstruction of the spherically averaged density profile for the seed of a halo having grown by PA can also be applied to a halo having suffered major mergers. This yields the spherically averaged density profile, $\langle\rho_{\rm p}\rangle(r_{\rm p})$, of a putative peak that would evolve by PA into a halo with a spherically averaged density profile identical, by construction, to that of the original halo. Clearly, if the halo has grown by PA, such a putative peak exists and it is an ordinary peak. However, if the halo has undergone major mergers, does it exist? Is it an ordinary peak? In which halo does it evolve? To answer these questions, we will make use of the rigorous treatment of the peak formalism given in MSSa and MSSb.

As mentioned, the peak ansatz at the base of the peak formalism states that there is a one-to-one correspondence between haloes with M at t and peaks in the filtered density field at some small enough cosmic time $t_{\rm i}$, for some monotonous decreasing and increasing functions $\delta(t)$ at $R_{\rm f}(M)$ of the respective arguments. According to this ansatz, peaks associated with *accreting* haloes describe continuous trajectories in the $\delta_{\rm pk}$–$R_{\rm f}$ diagram. Those peaks need not necessarily be anchored to points with fixed coordinates; they can move as the filtering scale varies (as real haloes do in the clustering process). However, thanks to the *mandatory* use of the Gaussian window,[13] the connection can be made in a simple consistent

---

[13] The decreasing behaviour of δ with increasing $R_{\rm f}$ implied by the growth in time of halo masses is only guaranteed for that particular filtering window (see MSSa).

way between peaks tracing one given accreting halo at contiguous scales.[14]

In a major merger, the continuous trajectories of (connected) peaks tracing the merging haloes are interrupted, while one new continuous peak trajectory appears tracing the halo resulting from the merger, leaving a finite gap in R_f due to the skip in halo mass between the merging and final objects. This is the only process where peak trajectories are interrupted. Haloes that do not merge but are accreted by more massive haloes are traced by peaks that do not disappear but become nested into the collapsing cloud of larger scale peaks tracing the accreting haloes. This leads to a complex nesting of peaks with identical δ_{pk} but different R_f. Once such a nesting is corrected, the number density of peaks with δ_{pk} at scales between R_f and $R_f + dR_f$ and its filtering evolution recover the mass function (and growth rates) of virialized haloes (MSSa and MSSb).

Thanks to these results, it can be shown (see MSSa) that the $\delta_{pk}(t)$ and $R_f(M)$ relations defining the one-to-one correspondence between (non-nested) peaks and (non-nested) haloes stated in the peak ansatz are necessarily of the form (37) and (38). These relations can be seen as the generalization of those of the same form found in top-hat spherical collapse, with $\delta_c(t)$ and q, respectively, equal to 1.686 and 1. This does not mean, of course, that these parameters must take the same values in the peak formalism. On the contrary, the freedom in $\delta_c(t)$ and q makes it possible to account for the change in the filtering window (Gaussian instead of top-hat) and possibly also in the departure from spherical collapse in the real clustering process.[15] For $\delta_c[t(z)] = 1.93 + (5.92 - 0.472z + 0.0546z^2)/(1 + 0.000\,568z^3)$ and $q = 2.75$, the halo mass function predicted in the ΛCDM concordance cosmology (after correction for nesting according to MSSa) recovers the mass function derived from the excursion set formalism from $z = 0$ up to any arbitrarily large z.[16] As the halo mass function at t predicted in the peak formalism is nothing but the filtering radius distribution for peaks with $\delta_{pk}(t)$ (equation 37) transformed into the former by means of the relation (38), this result implies that there is indeed a one-to-one correspondence between peaks and haloes as stated by the peak ansatz.

The putative peak of a halo and its associated peak according to the peak ansatz have the same $\delta_{pk}(t)$ and $R_f(M)$. Their filtering evolution may be different: the trajectory in the δ_{pk}–R_f diagram of the putative seed can always be traced down to any arbitrarily small filtering radius, whereas the trajectory of the associated peak can only be traced until reaching the filtering radius corresponding to the last major merger. However, the values δ_{pk} and R_f of a peak do not allow one to tell its 'past' filtering evolution because there is, in the filtering process, a kind of 'memory loss'. The Gaussian window, mandatory as mentioned for the peak formalism, yields a strong correlation between very close scales, which is welcome to carry out the connection between peaks at contiguous scales.

However, at the same time, it yields a loss of correlation between scales different enough to encompass the gap produced in major mergers. Thus, owing to this particular window, peaks at a given scale do not know whether or not they have appeared in some major merger (at a smaller scale). Therefore, the putative seed of a halo coincides with its associated peak according to the peak ansatz and, as such, it is an ordinary peak. (It contributes to the filtering scale distribution of peaks with a given δ_{pk}, regardless of the past history of the halo.)

Thus, according to the present model supported by the results shown in Section 5, the spherically averaged density profile of a halo having undergone major mergers must be indistinguishable from that arising from the evolution by PA of an ordinary peak (the putative peak) or, equivalently, there must be in the halo aggregation process a memory loss similar to that mentioned above, affecting the filtering process of peaks. Such an implication has to do with the fundamental debate on whether or not virialization is a real relaxation (e.g. Henriksen 2009).

As noted by Del Popolo et al. (2000), the one-to-one mapping between the initial and final density profiles in PA seems to indicate that there is no memory loss, at least in PA, during virialization. This is at odds, however, with the fact that virialization, even in PA, sets a time arrow. Even though the equations of motion of individual particles are time reversible, owing to the highly non-linear dynamics of shell-crossing, any infinitesimal inaccuracies in the positions and velocities of particles in a simulation are rapidly amplified, causing simulated orbits to deviate from the true ones. When the simulation is run forwards, this goes unnoted because the system always reaches the same (statistically indistinguishable) final equilibrium configuration. However, when the simulation is run backwards, it is readily detected: before shells can reach the maximum size (at turnaround), they begin to contract again towards the final equilibrium state. As the existence of a time arrow (or the impossibility of reversing by numerical means the evolution of a system) is an unambiguous signature of relaxation, we must conclude that virialization is a real relaxation.

In the case of PA, the memory loss on the initial conditions is not complete: the order of shell apocentres is conserved. Consequently, despite the fact that information regarding individual orbits is lost, we can recover the initial configuration in a statistical sense (in that we can recover the density profile). Thus, even in this case, the initial configuration cannot be *exactly* recovered because of the loss of information on the phase of particle orbits (individual orbits are mixed up). And, in the general case including major mergers, the relaxation nature of virialization is even more evident. The initial configuration of a given virialized object can never be recovered, not even in a statistical sense, because the density profile for virialized haloes does not harbour information on their past history, so we can never be sure that the unconvolved density profile of their putative seeds, derived assuming PA, describes the density profile of their real seeds.

The prediction made by the present model that the spherically averaged density profile of haloes does not harbour information on their past aggregation history is thus consistent with the general behaviour of virialization. Moreover, it is consistent with several specific results regarding the density profile of simulated virialized haloes: (i) virialized haloes with very different aggregation histories have similar spherically averaged density profiles (e.g. Nusser & Sheth 1999); (ii) their density profile is independent of the time they suffered their last major merger (Wechsler et al. 2002) and (iii) their density profile does not allow one to tell how many, when and how intense the major mergers they have suffered are (Romano-Díaz

---

[14] A peak at scale R_f is connected with another peak at scale $R_f + dR_f$ provided only these two peaks are at a distance smaller than R_f from each other (see MSSa).

[15] For this latter aspect to be true, we should adjust the mass function obtained from simulations or from the excursion set formalism, with values of δ_c and q better adjusting the former mass function. In the present paper, we fit, however, the mass function predicted in the excursion set formalism with $\delta_c(t) = 1.686$ and $q = 1$, so the departure from non-spherical collapse cannot be accounted for.

[16] The mass function predicted by the excursion set formalism is not fully accurate, particularly at large z, so one should rather fit the mass function drawn from numerical simulations. However, this is not important here.

et al. 2006). Certainly, there are also some claims in the literature that the density profile for haloes depends on their formation time. However, this is due to the particular definition of halo formation time adopted in those works, related to the form of the profile. Thus, the prediction of the model regarding the lack of information in the density profile of a halo on its past history is not contradicted by the results of numerical simulations.

Thus, the present model strongly suggests that haloes having suffered major mergers have density profiles which are indistinguishable from those that have not. This prediction is important not only for the validity of the model (i.e. the validity of the inside-out growth assumption and the peak ansatz), already supported by the good behaviour of the density profiles it predicts (Section 5), but also because it allows one to understand why major mergers do not affect neither the typical halo density profile nor the peak formalism for halo statistics based on SI. Indeed, the fact that haloes formed in a major merger, after complete virialization, would have a density profile indistinguishable from that of a halo formed by PA justifies that any halo with M at t can be associated with a peak with δ_{pk} and R_f as if it had evolved from it by PA, as assumed in the peak ansatz, and that the typical halo density profile derived assuming PA is not affected by major mergers. As a corollary we have that the present model of spherically averaged density profile should hold for all haloes, regardless of their aggregation history.

7 SUMMARY

The present model relies on two assumptions: (i) that the typical density profile for virialized objects in hierarchical cosmologies with collisionless dissipationless dark matter can be derived as if all the objects grew by PA and (ii) that the peak formalism correctly describes halo statistics. The key points of the derivation are that, contrarily to the kinematic profiles, the spherically averaged density profile does not depend on the (triaxial) shape of the object and that, during accretion, virialized objects grow from the inside out, keeping the inner structure essentially unchanged.

Triaxial collisionless dissipationless systems undergoing PA virialize by transferring energy from inner to outer shells through shell-crossing. Due to this energy loss, particles progressively reaching turnaround describe orbits that contract orderly in the sense that the ellipsoidal surfaces effectively traced by their apocentres shrink and change their axial ratios without crossing each other until they stabilize. This causes the central steady object to develop inside-out. Such an evolution of accreting objects is in full agreement with the results of numerical simulations.

One important consequence of the inside-out growth is that the radius encompassing a given mass in triaxial virialized objects formed by PA exactly coincides with the usual estimate of such a radius from the energy of the sphere with identical mass at turnaround. In this conditions, there is a one-to-one mapping between the density profile of the virialized object and its seed. This allows one to infer the typical spherically averaged density profile, $\langle\rho\rangle(r)$, of virialized objects from the energy distribution of their spherically averaged seeds, which can be calculated from the power spectrum of density perturbations making use of the peak formalism.

The consistency between the peak formalism and the one-to-one mapping between the initial and final density profiles following from PA implies that virialization must be a real relaxation. This conclusion agrees with the general behaviour of virialization (it sets a time arrow) as well as with specific results regarding the density profile of simulated haloes. As such, the spherically averaged density profile for haloes cannot harbour information on their past

aggregation history, which explains why major mergers do not alter the typical density profile of virialized objects derived under the PA assumption and do not invalidate the peak ansatz. In other words, the sole condition that virialization is a real relaxation is enough for the two assumptions of the model to be not only consistent but also fully justified.

The model has been applied to CDM haloes. We have derived the typical unconvolved spherically averaged density profile for peaks evolving by PA and from it the typical spherically averaged density profile for haloes with a given mass in a given epoch. Specifically, we have established the link between the typical halo density profile and the power spectrum of density perturbations in any given hierarchical cosmology. The typical halo density profile so predicted in the ΛCDM concordance cosmology is in very good agreement with the NFW and the Einasto profiles fitting the spherically averaged density profile of simulated haloes down to one-hundredth the total radius. However, such a theoretical profile does not have a central cusp. In the ΛCDM cosmology, the model predicts that simulations reaching increasingly higher resolutions will find a typical halo density profile that tends to a core (null asymptotic slope) which is slowly approached, even slower than current fits using the Einasto profile.

REFERENCES

Ascasibar Y., Yepes G., Gottlöber S., Müller V., 2004, MNRAS, 352, 1109
Avila-Reese V., Firmani C., Hernández X., 1998, ApJ, 505, 37
Bardeen J. M., Bond J. R., Kaiser N., Szalay A. S., 1986, ApJ, 304, 15
Bertschinger E., 1985, ApJS, 58, 39
Binney J., Tremaine S. D., 1987, Galactic Dynamics. Princeton Univ. Press, Princeton, NJ
Bond J. R., Myers S. T., 1996, ApJS, 103, 41
Bryan G. L., Norman M. L., 1998, ApJ, 495, 80
Crone M. M., Evrard A. E., Richstone D. O., 1994, ApJ, 434, 402
Dekel A., Devor J., Hetzroni G., 2003, MNRAS, 341, 326
Del Popolo A., Gambera M., Recami E., Spedicato E., 2000, A&A, 353, 427
Doroshkevich A. G., 1970, Astrofiz., 6, 581
Dubinski J., Carlberg R. G., 1991, ApJ, 378, 496
Efstathiou G., Frenk C. S., White S. D. M., Davis M., 1988, MNRAS, 235, 715
Einasto J., 1965, Trudy Inst. Astrofiz. Alma-Ata, 5, 87
Fillmore J. A., Goldreich P., 1984, ApJ, 281, 1
Frenk C. S., White S. D. M., Efstathiou G., Davis M., 1985, Nat, 317, 595
Fukushige T., Makino J., 1997, ApJ, 477, L9
Gao L., Navarro J. F., Cole S., Frenk C. S., White S. D. M., Springel V., Jnefins A., Net A. F., 2008, MNRAS, 387, 536
Ghigna S., Moore B., Governato F., Lake G., Quinn T., Stadel J., 2000, ApJ, 544, 616
Gott J. R., 1975, ApJ, 201, 296
Gunn J. E., 1977, ApJ, 218, 592
Gunn J. E., Gott J. R., 1972, ApJ, 176, 1
Hayashi E. et al., 2004, MNRAS, 355, 794
Helmi A., White S. D. M., Springel V., 2003, MNRAS, 339, 834

Henriksen R. N., 2009, ApJ, 690, 102

Hiotelis N., 2002, A&A, 382, 84

Hoffman Y., Shaham J., 1985, ApJ, 297, 16

Huss A., Jain B., Steinmetz M., 1999, ApJ, 517, 64

Jing Y. P., Suto Y., 2000, ApJ, 529, L69

Katz N., Quinn T., Gelb J. M., 1993, MNRAS, 265, 689

Komatsu E. et al., 2011, ApJS, 192, 18

Le Delliou M., Henriksen R. N., 2003, A&A, 408, 27

Łokas E. L., 2000, MNRAS, 311, 423

Łokas E. L., Hoffman Y., 2000, ApJ, 542, L139

MacMillan J. D., Widrow L. M., Henriksen R., 2006, 653, 43

Manrique A., Salvador-Solé E., 1995, ApJ, 453, 6 (MSSa)

Manrique A., Salvador-Solé E., 1996, ApJ, 467, 504 (MSSb)

Manrique A., Raig A., Solanes J. M., González-Casado G., Stein P., Salvador-Solé E., 1998, ApJ, 499, 548

Manrique A., Raig A., Salvador-Solé E., Sanchis T., Solanes J. M., 2003, ApJ, 593, 26

Merritt D., Navarro J. F., Ludlow A., Jenkins A., 2005, ApJ, 624, L85

Merritt D., Graham A. W., Moore B., Diemand J., Terzić B., 2006, AJ, 132, 2685

Mikheeva E., Doroshkevich A., Lukash V., 2007, Nuovo Cimento B, 122, 1393

Moore B., Governato F., Quinn T., Stadel J., Lake G., 1998, ApJ, 499, L5

Moutarde F., Alimi J.-M., Bouchet F. R., Pellat R., 1995, ApJ, 441, 10

Muñoz-Cuartas J. C., Macciò A. V., Gottlöber S., Dutton A. A., 2011, MNRAS, 411, 584

Navarro J. F., Frenk C. S., White S. D. M., 1997, ApJ, 490, 493

Navarro J. F. et al., 2004, MNRAS, 349, 1039

Navarro J. F. et al., 2010, MNRAS, 402, 21

Nusser A., 2001, MNRAS, 325, 1397

Nusser A., Sheth R. K., 1999, MNRAS, 303, 685

Peacock J. A., Heavens A. F., 1990, MNRAS, 243, 133

Peebles P. J. E., 1980, The Large-Scale Structure of the Universe. Princeton Univ. Press, Princeton, NJ, p. 64

Porciani C., Dekel A., Hoffman Y., 2002, MNRAS, 332, 325

Power C., Navarro J. F., Jenkins A., Frenk C. S., White S. D. M., Springel V., Stadel J., Quinn T., 2003, MNRAS, 338, 14

Quinn P. J., Salmon J. K., Zurek W. H., 1986, Nat, 322, 329

Raig A., González-Casado G., Salvador-Solé E., 1998, ApJ, 508, L129

Romano-Díaz E., Faltenbacher A., Jones D., Heller C., Hoffman Y., Shlosman I., 2006, ApJ, 637, L93

Ryden B. S., 1993, ApJ, 418, 4

Ryden B. S., Gunn J. E., 1987, ApJ, 318, 15

Salvador-Solé E., Solanes J. M., Manrique A., 1998, ApJ, 499, 542

Salvador-Solé E., Manrique A., Solanes J. M., 2005, MNRAS, 358, 901

Salvador-Solé E., Manrique A., González-Casado G., Hansen S. H., 2007, ApJ, 666, 181

Subramanian K., Cen R., Ostriker J. P., 2000, ApJ, 538, 528

Syer D., White S. D. M., 1998, ApJ, 293, 337

Tasitsiomi A., Kravtsov A. V., Gottlöber S., Klypin A. A., 2004, ApJ, 607, 125

Vera-Ciro C. A., Sales L. V., Helmi A., Frenk C. S., Navarro J. F., Springel V., Vogelsberger M., White S. D., 2011, MNRAS, 416, 1377

Wang J., White S. D. M., 2009, MNRAS, 396, 709

Wang J. et al., 2011, MNRAS, 413, 1373

Wechsler R. H., Bullock J. S., Primack J. R., Kravtsov A. V., Dekel A., 2002, ApJ, 568, 52

White S. D. M., Zaritsky D., 1992, ApJ, 394, 1

Williams L. L. R., Babul A., Dalcanton J. J., 2004, ApJ, 604, 18

Zaroubi S., Naim A., Hoffman Y., 1996, ApJ, 457, 50

Zeldovich Ya. B., 1970, A&A, 5, 84

Zhao D. H., Jing Y. P., Mo H. J., Börner G., 2009, ApJ, 707, 354

This paper has been typeset from a TEX/LATEX file prepared by the author.